THE ACOUSTIC RESULTS OF A UNITED TECHNOLOGIES SCALE MODEL HELICOPTER ROTOR TESTED AT DNW

Sandy R. Liu
Aerospace Engineer
U.S.Army Aeroflightdynamics Directorate (AVSCOM)
Moffett Field, California

Michael A. Marcolini
Research Engineer
NASA Langley Research Center
Hampton, Virginia

ABSTRACT

In a major cooperative program between U.S. Government agencies (represented by the U.S. Army Aeroflightdynamics Directorate and NASA Ames and Langley Research Centers) and United Technologies Corporation (represented by United Technologies Research Center and Sikorsky Aircraft Division), a 1/6 geometrically and aeroelastically scaled UTC model helicopter rotor was tested in the open-jet anechoic test section of the Duits-Nederlandse Windtunnel in the Netherlands. As the fourth entry under the Aerodynamic and Acoustic Testing of Model Rotors Program, several comprehensive acoustic and aerodynamic databases were obtained relating the important aerodynamic phenomena to both the near- and far-field acoustic radiation. In particular, high speed impulsive noise and blade-vortex interaction are of primary interest. This paper provides an initial summary of the acoustic measurements acquired for some of the different configurations tested. A review of the baseline swept tip rotor acoustic characteristics in the regimes of high speed forward flight, where high speed impulsive noise dominates, and low speed descent, where severe blade vortex interaction noise occurs, is presented. The trends of these primary noise sources are studied as the first step in validating the data for release and application.

INTRODUCTION

The increased use of helicopters in both civil and military applications has raised the awareness for the need to incorporate aircraft noise as a primary design parameter. In fact, the Federal Aviation Administration has enacted legislation requiring that newly designed helicopters meet stringent noise standards (Ref.1). With the increasing role of helicopters in the military, advances in the design of acoustic detection technology threaten operational effectiveness and jeopardises future missions. Consequently, the last decade has been committed to an intense helicopter aeroacoustics research effort, both to define the noise generating mechanisms and to examine means to reduce this noise (Ref.2-27). While computational methods continue to be developed, they have not yet matured to a level that will guarantee certification of a newly designed helicopter. As such, experimental research presently remains the critical ingredient necessary in establishing a firm understanding of the various sources of the rotorcraft noise problem. Therefore, in order to meet this challenge, in a joint effort of government and industry, the following test was performed.

The U.S. Army Aerodynamic and Acoustic Testing of Model Rotors (AATMR) Program, under the direction of the Aeroflightdynamics Directorate's Fluid Mechanics Division, was structured as a result of prior successful joint "Memorandums of Understanding (MoU)". Under an existing MoU between the United States and France, an AH-1/OLS scale model rotor was tested in the French CEPRA-19 Wind Tunnel (Ref. 2). Subsequently, the same rotor was tested in the Duits-Nederlandse Windtunnel (DNW) in the Netherlands, under another MoU between the United States and Germany (Refs. 3,4). It was this 'benchmark' test which led to the establishment of the AATMR Program between the United States government and the U.S. helicopter industry, in cooperation with the Dutch government. The main objectives of this program have been to investigate impulsive noise caused by blade-vortex interaction and high speed forward flight and

Presented at the 46th Annual Forum of the American Helicopter Society, Washington, DC May 1990

This is one of three papers in the 46th Forum on this test program. More detailed descriptions of the overall test and aerodynamic results are presented in the other two papers.

to obtain a fundamental understanding of the associated airloads, over a full range of flight regimes. The first industry participant was Boeing Helicopter Company, in a test involving a 1/5 size, dynamically scaled model of the Boeing Model 360 rotor. Simultaneous blade pressure and acoustic data were acquired over a full matrix of test conditions (Refs. 5,6). Data from this test complemented Boeing wind tunnel model scale data and full scale whirl tower and flight test data. In 1987, AFDD and McDonnell Douglas Helicopter Company, with NASA participation, tested a dynamically scaled model of the Hughes Advanced Rotor Program (HARP) composite bearingless model main rotor and a 369K tail rotor. This test focused on the acoustic characteristics, and also demonstrated an improved flexbeam design (Ref.7).

In 1984, United Technologies Research Center and the Sikorsky Aircraft Division of United Technologies initiated the design and fabrication of a densely instrumented model scale modern technology main rotor. An extensive series of hover tests were performed on this rotor in 1986-88 by a UTRC/Sikorsky team, as described in Refs.8-9. The hover test program included measurements of the blade pressures, strains and boundary layer state, rotor performance, wake geometry, and flow field velocities (using a laser velocimeter).

In an established trilateral rotorcraft testing effort at NASA Ames Research Center (ARC), structured for the correlation of model and full scale wind tunnel experiments and flight testing, NASA ARC, in cooperation with the Army, has scheduled a flight test of an instrumented full-scale rotor of the same design as the subject model in 1990. The pressure-instrumented main rotor system was fabricated by Sikorsky, and has many transducer locations in common with the model tested at DNW. The complementary and coordinated series of scale model wind tunnel tests and full scale flight tests will provide insight in the areas of acoustics, performance, aerodynamics, and dynamics. It is the model scale testing which will be discussed in this paper. An overview of the DNW test program is presented in Ref.10, and aerodynamic results are presented in Ref.11.

The subject test of the UTC model scale rotor at the DNW had the following objectives:

1) acquire blade airloads from pressure measurements over the entire extent of blade chord, span, and azimuth,
2) obtain simultaneous acoustics and blade pressure data over a wide range of operating conditions,
3) study main rotor/tail rotor interaction noise,
4) study near/far-field rotorcraft acoustics,
5) investigate wind tunnel shear layer effects on acoustic transmission, and
6) evaluate the acoustic and performance characteristics of a main rotor with a BERP-planform tip.

From an acoustic aspect, the main focus was on two of the dominant noise sources for rotorcraft: high speed impulsive (HSI) noise and blade- vortex interaction (BVI) noise. High speed impulsive noise is primarily a result of compressibility effects due to high advancing tip Mach numbers, as described in Refs. 12-13. Main rotor BVI noise is the primary noise source for rotorcraft in low-power descent, where the rotor wake is blown back into the rotor plane. Unsteady airloads are introduced on the blade by the close passage of one or more previously shed tip vortices. Because of the dependence of this phenomenon on the complex geometrical structure of the wake, its occurrence is extremely sensitive to rotor design and helicopter operating conditions (Refs. 14-16). Accurate prediction of BVI noise is required to reduce design margins currently needed to assure noise certification (Refs. 17-20).

To achieve these objectives, four different test configurations were used during the experiment:

1) baseline pressure instrumented main rotor
2) baseline uninstrumented main and tail rotors
3) baseline uninstrumented main rotor
4) BERP-planform tip uninstrumented main rotor

The composition of the configurations and of the test matrices will be discussed below. Each configuration focused on particular goals established and agreed upon in the early planning. All data presented in this paper are from the first configuration, so that configuration will be discussed in most detail here. Further details of the other configurations are contained in Ref. 10.

In the following sections, a description of the UTC scale model baseline rotor, the DNW wind tunnel, the acoustic data acquisition system, and test matrices are briefly discussed. Acoustic data are presented for three rates of descent and a comparison made of the sensitivity of BVI to this parameter. This is followed by an analysis and discussion of the high speed impulsive noise characteristics for high speed forward flight.

MODEL DESCRIPTION

Main Rotor and Hub

The baseline rotor used in this experiment is a 9.4 ft (2.9 m) diameter, 4-bladed scale (1:5.73) model of a current technology Sikorsky main rotor. The blades

have a joint at 80% of the radius to allow different tip designs to be tested. The baseline planform is shown in Figure 1; the primary distinguishing features are an effectively constant chord and a 20 degree aft sweep of the blade tip (beginning at r/R = 0.929). The average chord is 3.64 in (9.24 cm), producing a blade aspect ratio of 15.3 and a solidity of 0.0825. The Sikorsky cambered airfoils used for this rotor have a thickness-to-chord ratio of 0.095. The blade twist distribution is linear for r/R < 0.75 and nonlinear at the tip, with a maximum twist of -13 deg with respect to the blade root at r/R = 0.92. The blade geometry is completely defined in Refs. 8 and 9. The rotor system is shown installed at the DNW in Figure 2.

Two geometrically identical versions of the baseline rotor were tested: an 'uninstrumented' rotor, which contains only strain gages, and an 'instrumented' rotor, which contains pressure, strain, and temperature sensors. Blade structural and dynamic characteristics are provided in Ref. 9, including stiffnesses, mass distributions, inertial properties, and natural frequencies (as determined by non-rotating rap tests). Structural properties of the uninstrumented baseline rotor closely match the full scale rotor. The addition of the pressure transducers, the associated electronics and supports raises the mass of the instrumented rotor to approximately 30% above the scale value.

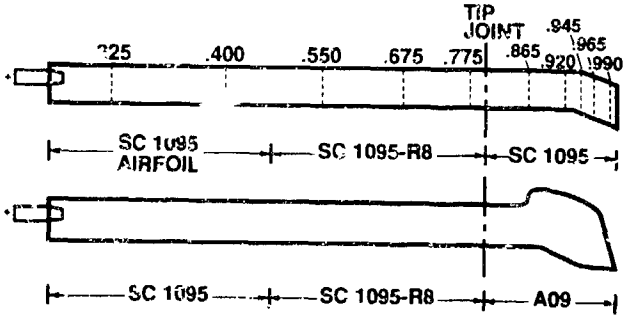

Figure 1. Planforms of UTC model main rotors.

For this test the model blades were mounted on a Sikorsky fully-articulated rotor hub. The hub has a hinge offset of r/R = 0.053, coincident flap and lag hinges, and viscous lag dampers to avoid inplane mechanical instabilities. Potentiometers on the rotor head measured blade motion angles (pitch, flap, and lead-lag). Strain gages measured loads on the four pitch links.

Test Stand and Balance System

The UTC model rotor and hub were mounted on the AFDD's Rotary Wing Test Stand (RWTS). The test stand is comprised of four major subsystems: the electric drive motors, the transmission, the rotor balance system, and the rotor control swashplate system. A 1024 encoder and optical 1 per rev encoder were used to control the clock rates and trigger for the online digital acoustic data acquisition system, respectively. The swashplate and RWTS were enclosed for this test with acoustic fairings. These consisted of fiberglass shells covered with acoustic, sound absorptive foam. The RWTS was directly attached to the DNW sting support system, which was also covered with a sound absorptive foam fairing. In this test, all degrees of freedom of the sting except for the shaft angle, α_s, were mechanically locked out. Additional details of the test stand are contained in Ref. 10.

Figure 2. UTC main and tail rotor at DNW.

TEST FACILITIES

The German-Dutch wind tunnel, the DNW, is a cooperative establishment of the aerospace research laboratories Deutsche Forschungsanstalt fur Luft-und Raumfahrt (DLR) in Germany, and the Nationaal Lucht-en Ruimtevaartlaboratorium (NLR) in the Netherlands. This joint venture was a milestone for international cooperation in the field of aeronautics. Officially opened in 1980, DNW is Europe's largest and most versatile wind tunnel, and has outstanding aerodynamic and aeroacoustic properties. Figure 3 shows an aerial view of the facility. By offering the aeroacoustic features of low background noise, a large anechoic testing hall, and both in-flow and out-of-flow microphone traverse systems, the DNW has become a major rotorcraft testing facility (Ref. 21).

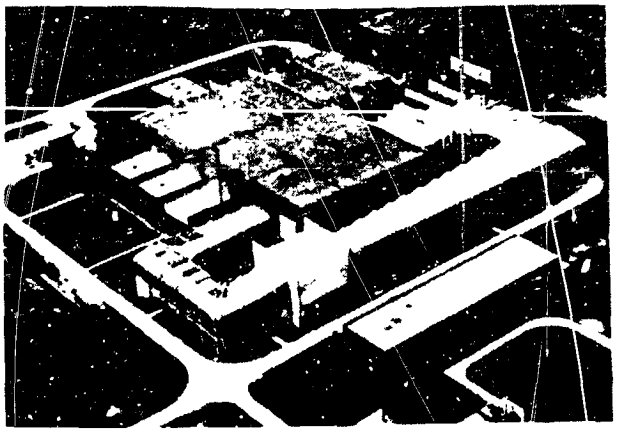

Figure 3. The aerial view of DNW wind tunnel facility.

The DNW is a subsonic, atmospheric wind tunnel of the close- return type . It has three interchangeable closed test section configurations and one open-jet configuration with a 6.0 by 8.0 meters (19.7 by 26.2 ft) nozzle. All data for this program were acquired in the open-jet configuration, where flow velocities of up to 80 m/s (262.5 ft/sec or 155 kts) can be reached, which covers the typical speed range of existing helicopters. The tunnel was designed for low background noise by choosing a low-tip-speed fan and by acoustically lining the turning vanes and collector/transition walls. An acoustically treated testing hall of more than 30,000 m^3 (52 x 20 x 30 m) surrounds the open-jet testing configuration, much of which is usable for in-flow or out-of-flow acoustic measurements. The exceptional anechoic properties (cutoff frequency of 80 Hz) which result make the DNW the largest aeroacoustic wind tunnel in the free world. The tunnel also has excellent fluid dynamic qualities with low unsteady disturbances over the total testing velocity range. More detailed information of the tunnel characteristics can be found in the Appendix of Ref.3. Further DNW information can be found in Ref. 22.

The UTC model rotor was positioned on the vertical and lateral centerline of the DNW test section, and aft 1.86 meters (6.1 ft) from the longitudinal centerline. This position enabled acoustic measurements to be made 3.0 rotor diameters upstream of the hub, as required for direct comparison with earlier DNW test results (Ref.2,3,5,6). The vertical position of the rotor hub center was maintained at the tunnel centerline for all shaft angles by raising and lowering the sting.

INSTRUMENTATION SYSTEMS

Signal conditioning, data acquisition, display, and processing hardware for this test were located in two transportable instrumentation trailers supplied by the Army. Two data acquisition systems were used: an AFDD system for acoustics and performance data and a UTRC system for rotor aerodynamics, dynamics, and performance. A third computer, supplied by NASA Langley, was used for additional acoustics data processing. The data acquisition systems were installed in the trailers and checked out at NASA Ames Research Center prior to the DNW entry. Following is a detailed description of the acoustic systems used. Details of the airloads acquisition system will not be addressed but can be found in References 10 and 11.

AFDD Acoustic/Performance/Control system

Rotor and strain gage data were recorded on analog tape. Performance data from the balance and wind tunnel parameters were digitized at 300 Hz, processed on line by a VAX 11/751 computer, and stored on magnetic tape. An analog backup tape of this data was recorded as well. Fifteen in-flow and four out-of-flow microphones were used to measure the acoustic pressure. This information was recorded on analog tape, as well as digitised with a DATACOM A-to-D front end to the VAX 11/751. The digitised data were processed, and instantaneous and averaged time histories as well as FFT spectral plots were available on site.

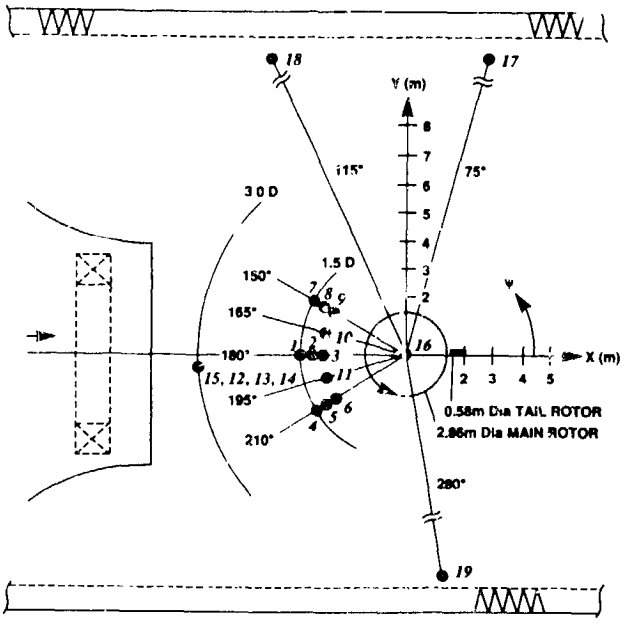

Figure 4. Microphone positions in DNW (top view).

The acoustic acquisition system, consisting of nineteen microphones, was divided into arrays of in-flow and out-of-flow positions relative to the wind tunnel jet stream. Eleven microphones, numbers 1 - 11, were mounted on the DNW movable in-flow traverse, upstream of the rotor, and two microphones, 17 - 18, were attached to an out-of-flow traverse, located on the wall

of the test section, as seen in Figure 4. Four microphones, numbers 12 - 15, were mounted in a fixed, inflow array just downstream of the nozzle exit, as shown in Figure 5. Microphones 16 and 19 were fixed to the ceiling and wall of the test section, respectively, as can be seen in Figure 6. The microphones were arranged on radials from the rotor hub, both in plane and below the rotor disk. Microphones 1 - 11, located on the inflow traverse, were 1.5 diameters away from the rotor hub. To maintain this separation distance when the shaft was tilted for each particular test condition, the inflow array would move upstream or downstream.

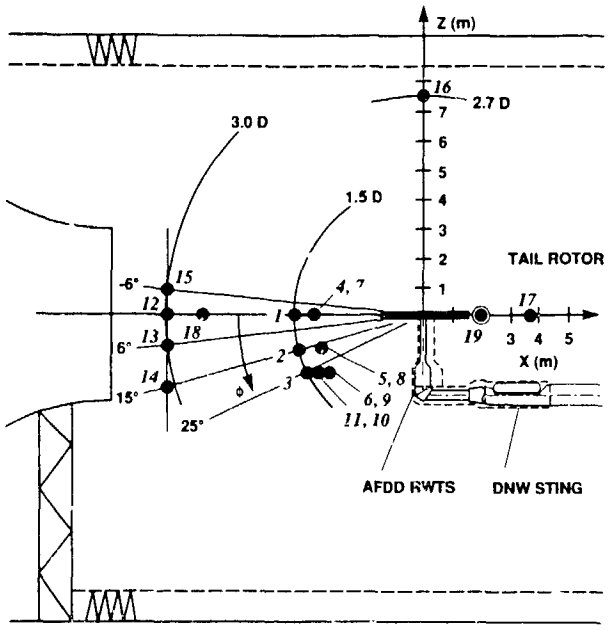

Figure 5. Microphone positions in DNW (side view).

All in-flow microphones (numbers 1 - 15) were standard B&K 4134 1/2 inch pressure type condenser microphones equipped with "bullet" type nose cones. The out-of-flow microphones (numbers 16 - 19) were B&K 4133 1/2 inch condenser microphones fitted with acoustic foam ball wind screens. Each microphone channel, consisting of the microphone, preamplifier, and power supply, was calibrated daily using a 124 dB at 250 Hertz sine wave pistonphone signal. In addition, a white noise and sine wave signal was frequently injected using the insert voltage calibration technique to check the system integrity over the course of the test.

Signal conditioning of the microphone signals were performed by amplifier/filter units. Acoustic data were filtered at 10 kHz with a six pole Bessel filter with 36 dB per octave terminal slope. Amplifier and filter settings were read and recorded digitally with the VAX

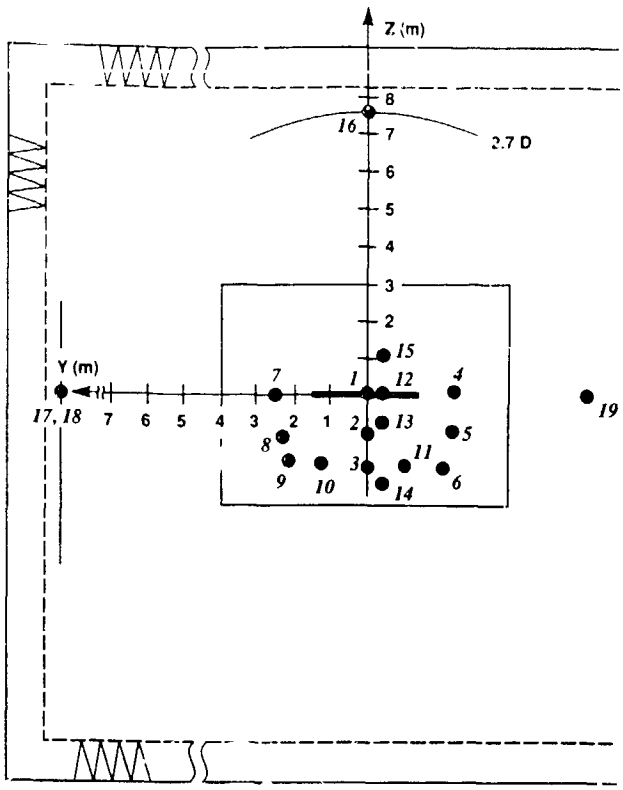

Figure 6. Microphone positions in DNW (front view).

11/751 data acquisition computer. Each file of acoustic data was stored with corresponding amplitude and filter information, as well as rotor performance characteristics. Data was digitized by a 15-bit (14 plus sign) DATACOM analog-to-digital(A-to-D) unit controlled by the VAX 11/751. Dynamic range of 90 dB was achieved with the 15-bit system. With amplifier gains set to prevent clipping, 85 dB dynamic range should be assumed for acoustic data digitized on line. The A-to-D was designed for a sample rate of approximately 400,000 samples per second. Analog-to-digital controller hardware buffer memory had a maximum size 2,641,440 16-bit words. The 19 microphones were digitized at 1024 samples per rotor revolution for 64 revolutions (approximately 2.26 seconds). Six microphones at a time were digitized simultaneously in three sequential groups, with a group of five microphones following. The VAX 11/751 computer controlled the A-to-D converter, stored calibration data, amplifier gains, filter settings and acoustic data, and performed time domain and spectral analysis.

A VAXStation 3200 computer, provided by NASA Langley, aided in the postprocessing of the digitized data files. Because of the large quantity of acoustics data, it was decided to transfer the digitized files

to the VAXStation 3200, to take advantage of its increased processing speed (relative to the VAX 11/751), and thereby obtain preliminary acoustic results more quickly.

Acoustic data were recorded on a thirty-two channel analog tape machine simultaneously with the digitization of the data. Timing and synchronization signals such as main rotor 1 per rev and 1024 per rev were recorded, as was a voice channel identifying test point number and test condition. The 1 per rev was recorded on two adjacent tape channels to eliminate the effects of phase shift between the odd and even recording heads. The 1024 per rev was recorded with a direct card, due to its very high frequency content, while all other channels were recorded with FM cards. Analog tape data were recorded on Wide Band I at 76.2 cm/sec (30 inches per second (IPS)) tape speed, giving a flat frequency response to 20 KHz for the FM-recorded signals. Dynamic range for this machine and intermediate band recording system was specified to be 48 dB, and it was measured to meet or exceed that specification. With amplifier gains set to prevent inadvertent clipping, it can be assumed that acoustic data were recorded with at least 45 dB dynamic response.

The analog pressure signals from the blade transducers were also supplied to the AFDD data system. One test objective was to correlate instantaneous (same rotor revolution) blade pressure and acoustic data for a limited number of test conditions. This correlation required that both the blade surface and acoustic pressures be simultaneously recorded by a single system. Therefore, the 22 blade pressure signals were passed to the AFDD system and recorded simultaneously with a select subgroup of five microphone signals on analog tape. The recording was repeated for each of the eight multiplexer positions.

TEST CONDITIONS

Four rotor configurations were tested during this experiment. The initial and primery configuration was the UTC pressure instrumented baseline main rotor, where the major emphasis was on obtaining a comprehensive mapping of the 176 blade surface pressures together with simultaneous acoustic field pressure measurements. Data analysis to date has concentrated on this configuration, which will be described in detail here. A description of the test conditions for the other three configurations is contained in Ref. 10.

Pressure Instrumented MR Configuration

For this configuration, the main portion of the test, 42 separate level flight conditions, 43 descent conditions, 5 high negative shaft angle (broadband noise) conditions, and 19 hover conditions were tested. The level flight conditions included advance ratios of 0.07 to 0.36, hover tip Mach numbers between 0.6 and 0.7, and thrusts of C_L/σ from 0.04 to 0.10. Descent conditions consisted of 9 shaft angle sweeps at 7 different advance ratios between 0.137 and 0.3. Figure 7 shows the instrumented main rotor in the DNW test section. The combined measurement of the blade surface pressures and the acoustic field provided a very high fidelity data base for aeroacoustic cause and effect studies.

Figure 7. Pressure instrumented main rotor in DNW.

ACOUSTIC TEST RESULTS

The following discussions of BVI and HSI noise will focus on the preliminary analysis of the UTC baseline swept tip rotor acoustic data. Several comparisons are made relative to the AH-1/OLS rotor (Ref 2,4,12-14) since the BVI and the HSI acoustic sources have been thoroughly analysed and because it identifies many fundamental phenomena associated with helicopters. The ranges of the four governing nondimensional parameters studied in the analyses presented are as follows:

Advancing tip Mach number, M_{AT}: 0.550 - 0.93

Hover tip Mach number, M_H: 0.550 - 0.700

Advance Ratio, μ: 0.100 - 0.328

Thrust coefficient/solidity, C_t/σ: 0.050 - .100

Shaft tilt angle (TPP angle), α_s: 0.05 - 7.47

Acoustics Repeatability of Check Points.

The excellent aerodynamic flow quality and acoustic properties of the DNW contribute to both the steadiness and superb repeatability of the acquired acoustic data. Over the course of the testing, defined check points were taken to insure the reliability and

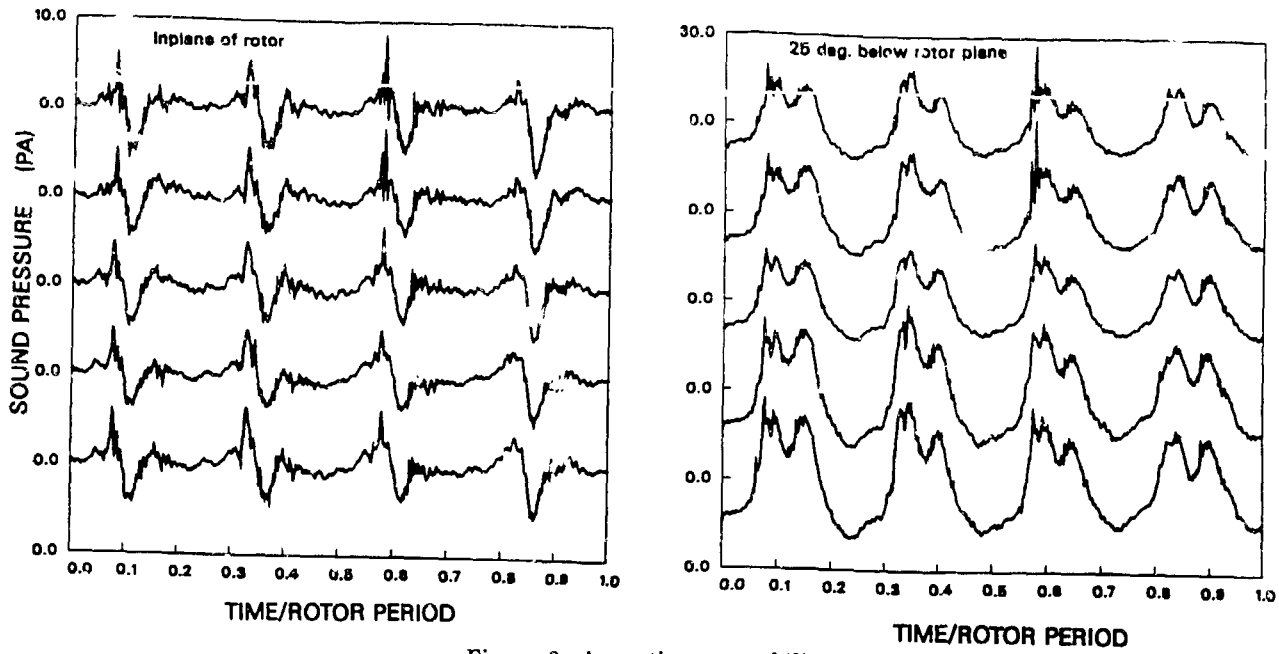

Figure 8. Acoustic repeatability.

repeatability from day to day. For the instrumented rotor, Figure 8 shows acquired acoustic time histories for a low speed forward flight case taken on different days, both inplane and 25° below the rotor, 1.5 rotor diameters from the hub. The repeatability is excellent considering the flight condition was a case involving substantial wake interactions (as revealed by the measured blade surface pressures). It is noted that there is more variation between the blade to blade signatures than that from day to day, which indicates that the repeatability of test points is at worst on the order of the variations between blades, and is possibly better than that. For a matching operational test condition, the time histories of the uninstrumented rotor matched well against the instrumented rotor, indicating that the pressure instrumentation has little to no effect on the acoustics. Therefore, mixing performance and acoustics data for these two blade sets is a valid way to establish data trends for the baseline planform.

Blade-Vortex Interaction (BVI) Data.

Blade-vortex interaction noise (BVI) is due to the shed tip vortex from a preceeding blade colliding with, or passing very near, a following blade. This collision produces an impulsive signature due to the rapid pressure changes at the leading edge of the rotor blade, and is a dominant noise source primarily in descent. BVI also exhibits a highly directional radiation pattern, with the major lobe of this pattern being forward of the blade, normal to its position at the time of the interaction, and below the rotor plane (Ref. 3).

In an effort to examine this model scale data from the perspective of comparing to future full-scale flight data with this same rotor design, it is necessary to evaluate the BVI characteristics as related to the normal rotor operational flight parameters, and gain a physical understanding of the nature of the BVI with respect to this rotor design. Since BVI is dominant during descent, the first step in the analysis was to define typical approach patterns and relate these to the measured test points acquired. This required transforming one of the governing scaling parameters used in the wind tunnel, shaft tilt angle (or tip-path-plane angle), into the more used piloting metric, rate of climb (in this case, rate of descent). A set of preliminary rate of descent calculations was performed by Sikorsky Aircraft Division using a generalised helicopter simulation program to relate the model shaft tilt angle to a typical rate-of-descent. In doing so, the approximate relation between shaft tilt angle (synonymous to tip-path-plane angle here since the rotor was trimmed for zero flapping) and rate of descent is plotted versus advance ratio in Figure 9. Note that the shaft tilt angles have been normalised by the shaft tilt angle value for a normal approach at μ=0.2. The calculated descent rates are 400, 600 and 800 ft/min shown by the smooth curves. The measured data, represented by the individual symbols, fall within the envelope of interest. From the measured acoustic data, three approach maneuvers at a fairly constant rate of descent could be simulated. The three approach rates chosen for this analysis are: a shallow approach of 400-500 ft/min represented by the solid circles, a normal approach of 600-650 ft/min represented by the

open circles, and a steep approach of 800-850 ft/min represented by the solid squares.

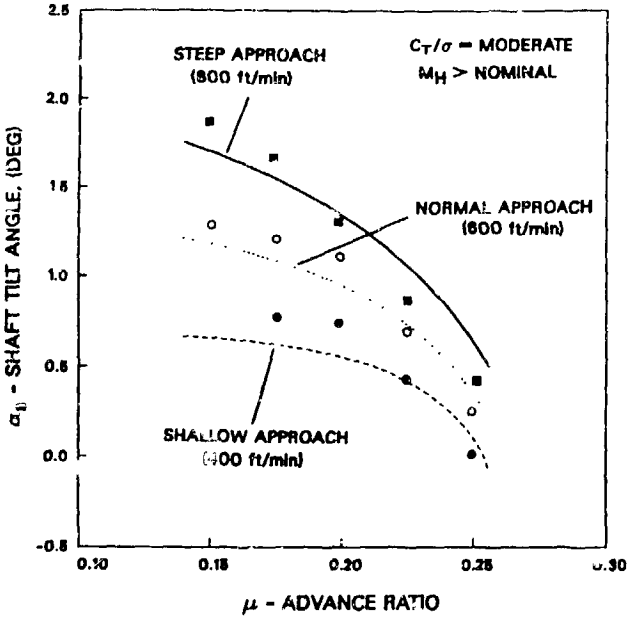

Figure 9. Descent Maneuver Matrix.

Because of the known forward-and-below directivity of BVI, data from the array of microphones (numbers 5,11,10,9) stationed 1.5 diameters away from the rotor hub in a plane 25 degrees below the tip path plane will be examined. These microphones correspond to positions at ψ= 210°, 195°, 165°, and 150°, respectively. These measurements identify the forward BVI directivity patterns and levels as the rotor performs the three selected approach maneuvers.

Figures 10a-10d show a portion of the measured acoustic pressure time histories from each of the four microphones at a given advance ratio for the three constant rate of descent maneuvers of 400-500 ft/min, 600-650 ft/min and 800-850 ft/min. Advance ratios of μ =0.15, 0.175, 0.20, and 0.25 are presented in Figures 10a through 10d, respectively. In Figure 10b, for μ=0.175, the directionality of BVI as a function of rate of descent is most clearly seen. At the shallowest descent rate of 400 ft/min, there is some evidence of BVI impulses at all of these forward microphone positions. Going from 400 ft/min to 800 ft/min, the BVI impulses are concentrated in the ψ =150° and ψ =165° locations. This indicates that, as the rotor shaft angle is increased, providing a steeper rate of descent, the vortex interactions move further back in the first quadrant. This produces the change in directivity, with the BVI lobe moving more to the right of the rotor. These results have also been seen by Martin (Ref. 23) in another rotor test at DNW.

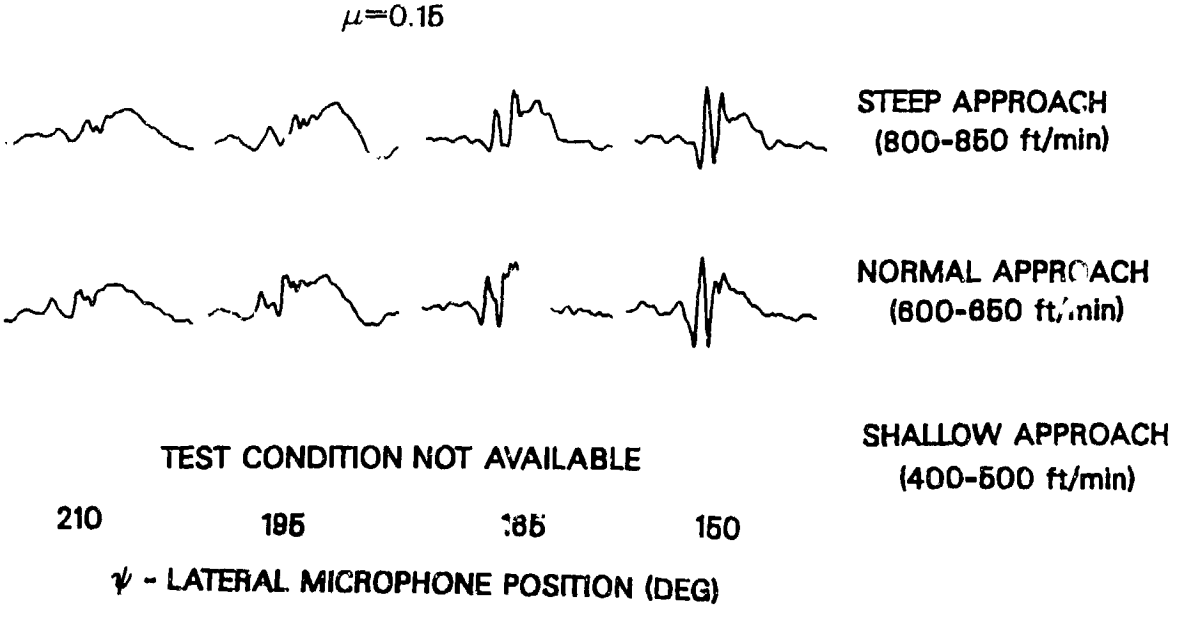

Figure 10a. BVI acoustic pressure time history (1/4 Rev) for descent at μ=0.150.

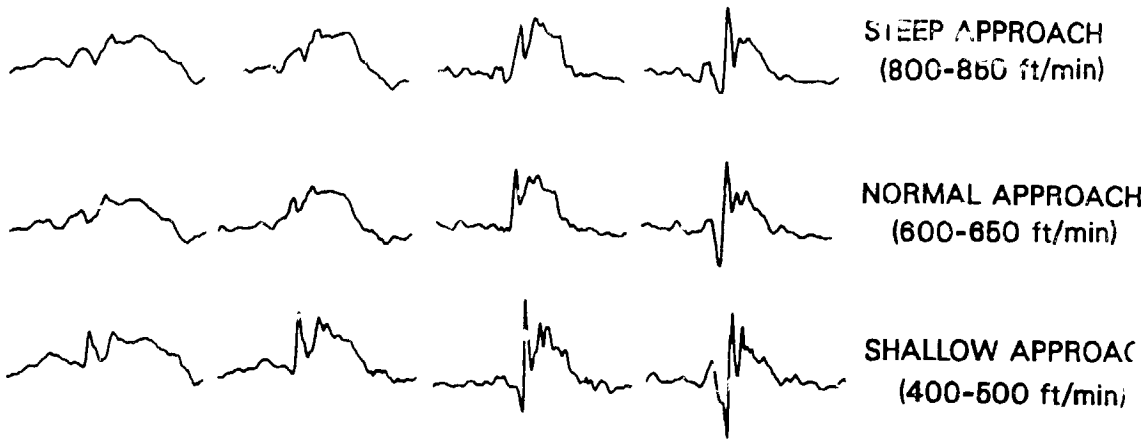

Figure 10b. BVI acoustic pressure time history (1/4 Rev) for descent at μ=0.175.

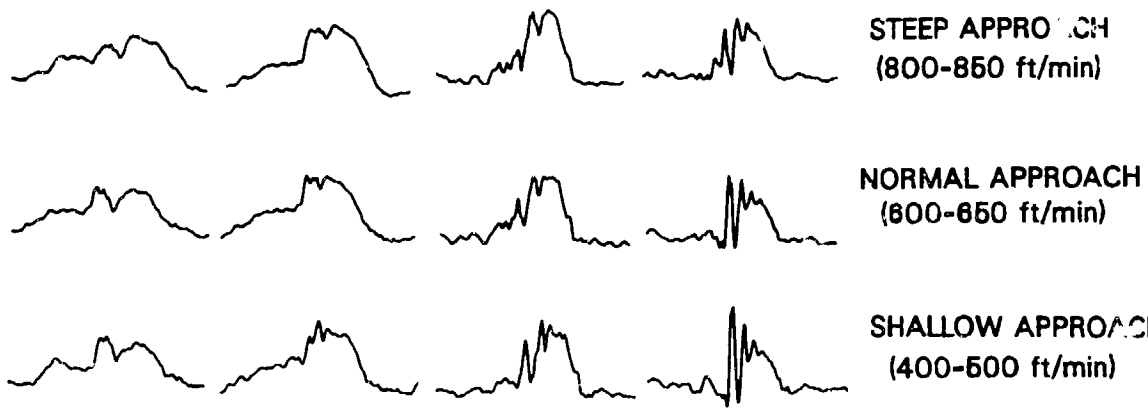

Figure 10c. BVI acoustic pressure time history (1/4 Rev) for descent at μ=0.200.

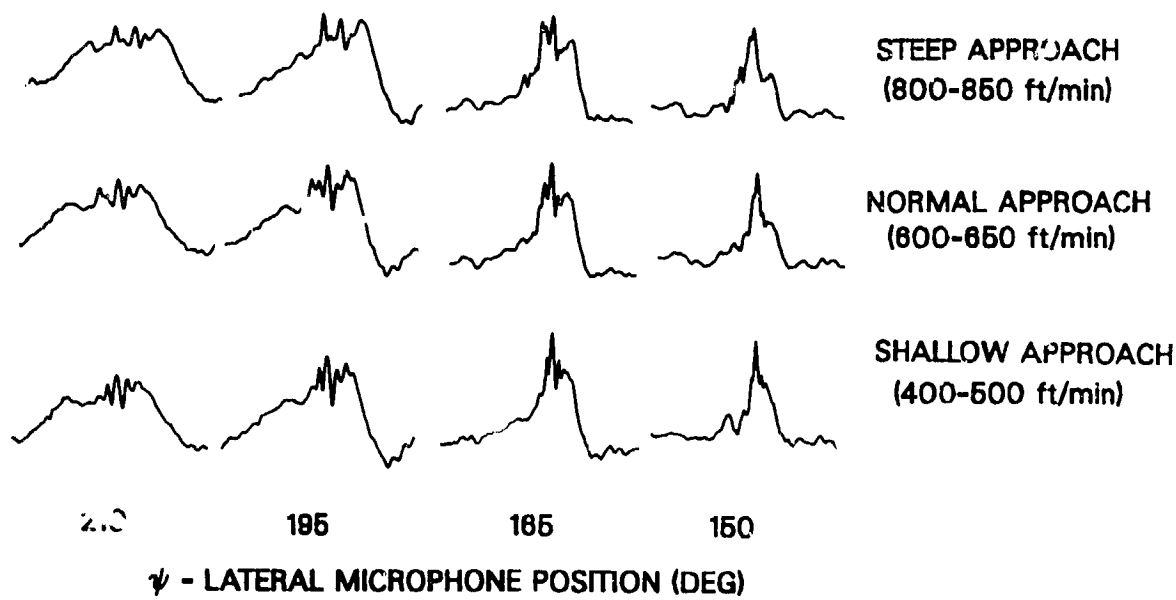

Figure 10d. BVI acoustic pressure time history (1/4 Rev) for descent at μ=0.225.

Examining Figures 10a, 10c, and 10d, similar trends are seen. The BVI directivity at the lowest descent rate is mostly forward of the rotor, and as descent rate is increased, the BVI tends to move toward the right. In addition, it should be noted that the BVI noise pulse shape changes in character at the same time. At the shallowest descents, the BVI impulses are much sharper, while they become broader, with lower amplitudes, as descent rate is increased. In addition, for the shallow and normal approaches, there are a number of discrete peaks, indicating the influence of as many as five shed tip vortices. This becomes less apparent in the steep approach, indicating a reduced number of interactions at higher rates of descent. It is likely that the increased vertical velocity component is causing the wake to pass through the rotor disk more quickly, both reducing the number of direct interactions with the blade, as well as moving those interactions that do occur further back on the rotor disk. This would produce both the directivity changes seen, as well as the shape of the BVI impulses. This would indicate that, for the steeper descents, the main BVI directivity location is to the right of the ψ =150 ° microphone location.

In a preliminary evaluation of the vortex interaction locations, the tip vortex geometry pattern based on a simple rigid wake was calculated. Figure 11 is calculated for the test condition of μ= 0.176 at a shallow approach, which is the test case from Figure 10 with the highest peak to peak acoustic pressure. The depicted intersections agree fairly well with preliminary measured blade pressure data at this condition, which are unfortunately not available for publication at this time. Figure 11 indicates interactions occurring at: ψ = 6 °, 22 °, 34 °, 45 °, 55 ° and 63 °. The fourth and fifth interactions are parallel to the blade at the time of interaction, with the vortex sweeping the blade from outboard inward. Data from the AH-1/OLS rotor (Ref.17) show parallel interactions with this same type of motion, and also show that the local pressure fluctuations due to these interactions were small at outboard stations but increase at inboard stations. In the other interactions, the vortices interact with the blade at oblique angles which sweep the blade from outboard inward. It is interactions of this type, an oblique interaction, which cause the resulting radiation to propagate perpendicular to the Mach cone around the trace of the disturbance along the vortex trajectory (Ref.24). By applying the equations from Ref.24, a very simple way of identifying the direction of radiation from oblique interactions was possible.

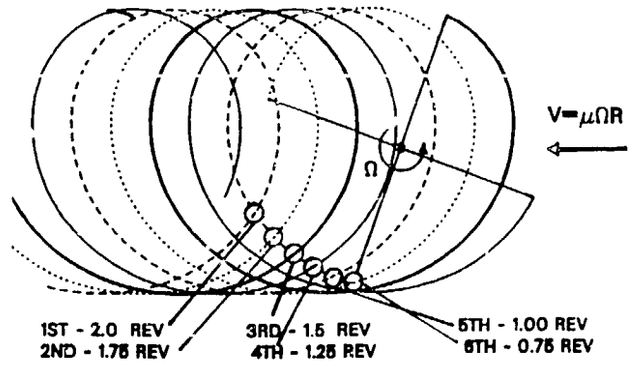

Figure 11. Rigid wake tip vortex geometry pattern.

Realizing that the early vortex interactions (first and second) are not likely to radiate in the measured area of interest, it seems possible that the BVI impulses seen for the test case (μ= 0.176), in Figure 10b, may be due to the third, fourth, fifth, and sixth interactions. Similarly, assuming that the parallel interaction mechanism acts ideally like that of the AH-1/OLS rotor, the primary radiation of the third and fourth interactions would be starboard, almost perpendicular to the blade at the time of complete interaction. Simple geometrical calculations indicate that the dominant peak seen is most likely the result of the fourth interaction occurring at ψ = 45 °, followed by the weaker effects of the fifth and sixth interactions. The fourth interaction has a radiation directivity of ψ=135 ° and is the dominant interaction pulse primarily on the advancing side as shown in Figure 10b. Although the third interaction is also a parallel interaction with a trace Mach number also equal to infinity, its radiation directivity is at ψ=145 ° which is almost out of the range of the measuring array. Nevertheless, there is evidence of it in Figure 10b, as the weaker pulse preceding the fourth interaction pulse in the measurements at ψ =150 °. These measurements seem to correlate well with the simple reasoning used for the known BVI mechanisms' radiation directions. With further analysis, using both acoustic prediction codes and the input of the measured blade pressure data, the following preliminary observation can clearly be confirmed and the mechanisms further studied.

In addition to examining the changes in the time history characteristics, overall and band limited sound pressure levels (OASPL and BLSPL) were calculated. Since BVI noise dominates the mid-frequency range and overall sound pressure levels are usually dominated by low frequency levels, a range between 500 Hz and 5 kHz was selected to identify the effects of BVI. For the overall sound pressure levels, the frequency ranged from 0 - 10 kHz.

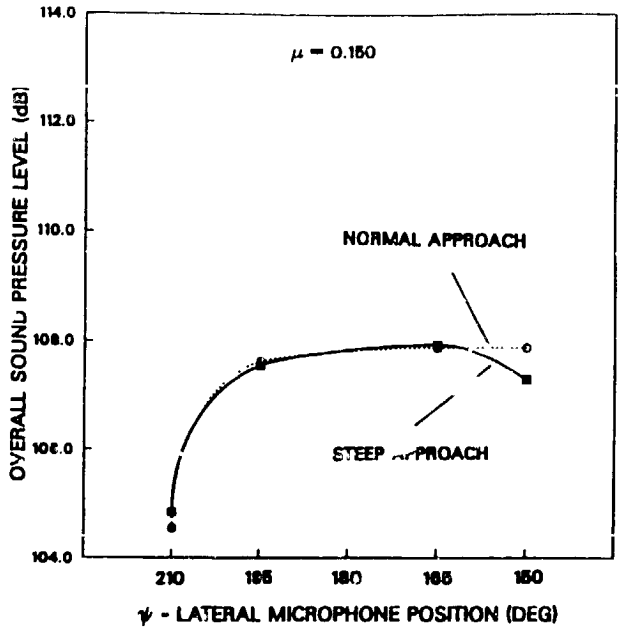

Figure 12a. Overall sound pressure level Directivity for descent at μ=0.150.

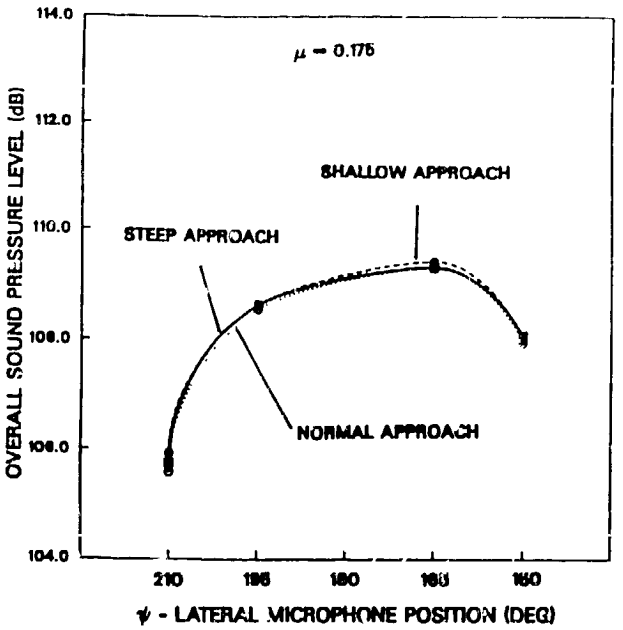

Figure 12b. Overall sound pressure level Directivity for descent at μ=0.175.

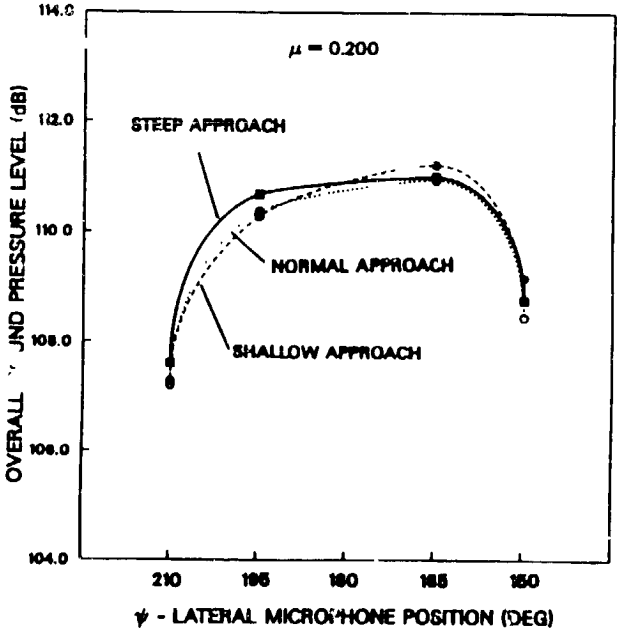

Figure 12c. Overall sound pressure level Directivity for descent at μ=0.200.

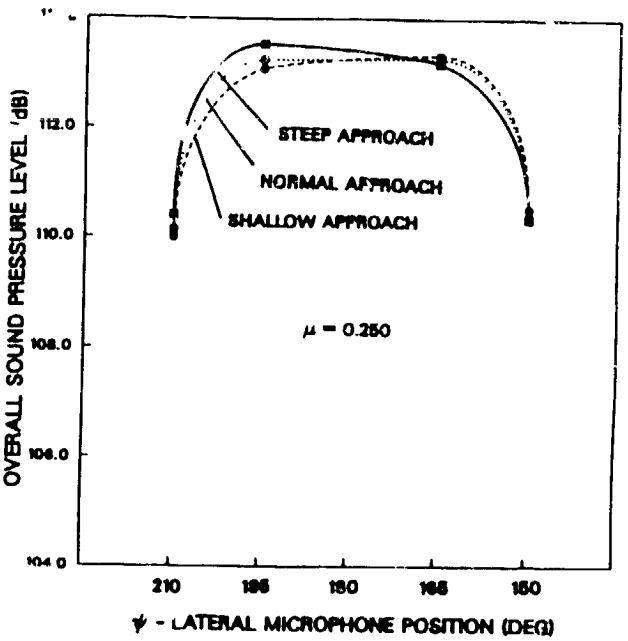

Figure 12d. Overall sound pressure level Directivity for descent at μ=0.250.

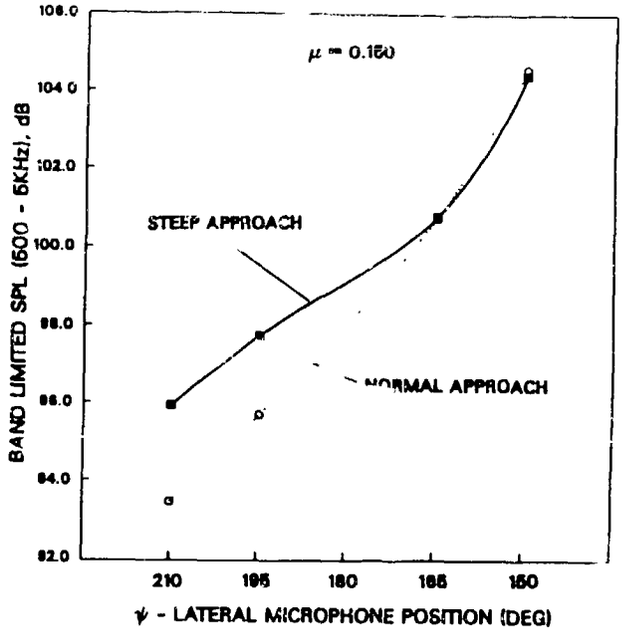

Figure 13a. Band limited sound pressure level Directivity for descent at μ=0.150.

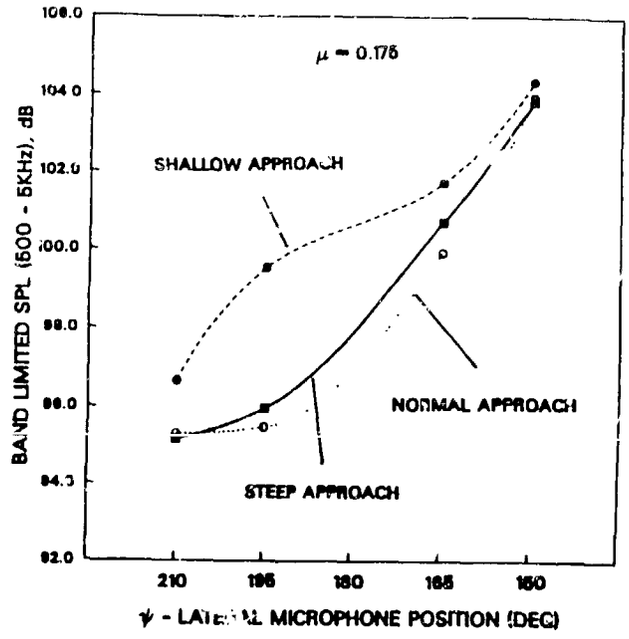

Figure 13b. Band limited sound pressure level Directivity for descent at μ=0.175.

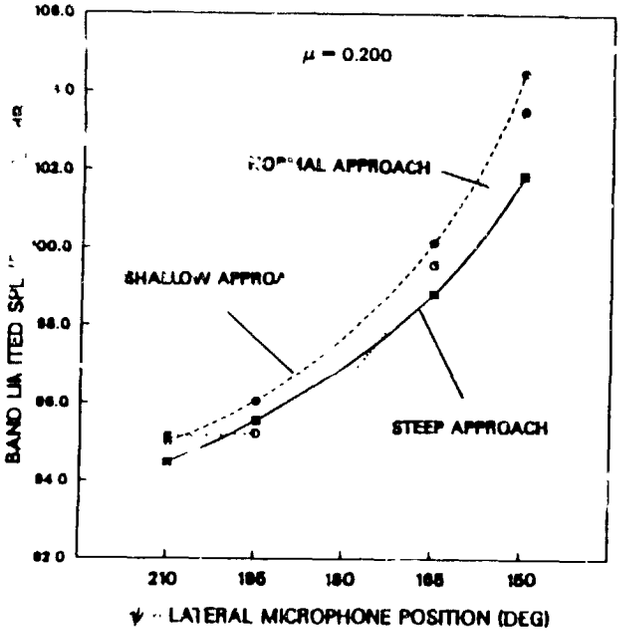

Figure 13c Band limited sound pressure level Directivity for descent at μ=0.200.

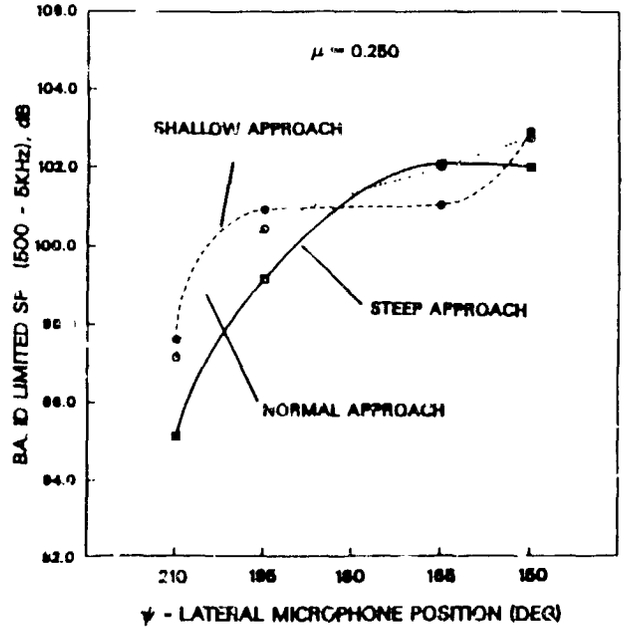

Figure 13d. Band limited sound pressure level Directivity for descent at μ=0.250.

In Figures 12a-12d, OASPL is plotted for the corresponding test conditions of Figures 10a-10d. This identifies the directivity of the summed total of all sound sources for a given μ at each of the three approach maneuvers. In Figure 12a, for μ =0.15, it is evident that there is little difference in the directivity and levels between OASPLs of the three different approaches. This says that for a given μ, the effects of shaft tilt are very weak. The only exception is at the advancing side microphones, where there is a slight increase in OASPL at the highest descent rate. This is due to the increasing role of BVI as a dominant noise mechanism. Similar trends are seen in the remainder of Figure 12.

In order to clearly evaluate the sensitivity and directivity of the BVI noise for each of the approaches, Figures 13a-13d show the BLSPL versus the microphone lateral position with each curve representing an approach test condition. Throughout Figure 13, a far greater sensitivity in the lateral directivity is seen, due primarily to BVI. The highest levels are consistantly on the advancing side for the majority of all the approach test conditions. A maximum difference of 10 dB is shown between the advancing and retreating side in each of the approaches. In addition, the 400 ft/min descent rate tends to produce the highest levels at the two microphone locations at ψ =195° and ψ =210°, which provides further indication that the BVI directivity is moving to the right as descent rate is increased. This shows that any small azimuthal (yaw angle) variation in flight path during full-scale descents can produce significant changes in the measured noise field.

High Speed Impulsive (HSI) Noise

As a rotor blade moves through the air, the finite blade thickness forces the air around the leading edge, which then rushes in at the rear of the blade, producing an impulsive noise source referred to as thickness noise. This noise radiates a large negative pressure pulse forward of the direction of blade motion, and is most dominant in the rotor tip-path-plane. In addition, as the advancing tip Mach number M_{AT} increases to transonic speeds, quadrupole sources around the blade become potent noise generators, particularly when extensive shocks are present due to the phenomenon of delocalisation. The resulting noise, known as high speed impulsive (HSI) noise, has a similar radiation pattern as thickness noise, and is shock-like in nature, i.e. sharp pulses of pressure propagating to the far-field. These mechanisms will now be examined for the current data.

Figure 14 shows results for a typical range of level forward flight conditions, examining the effects of increasing advance ratio on impulsive noise. These are measurements of microphone #1, which is stationed in the rotor plane at ψ= 180°, where high speed impulsive noise is supposed to dominate. In the central portion of the figure, the solid and open symbols represent a moderately and highly loaded rotor, respectively, both operating at the same propulsive force coefficient. It shows the expected increasing trend of negative peak acoustic pressure for higher advance ratio relating to the onset of high speed impulsive noise. These two curves nearly collapse, revealing that the negative peak pressure is relatively insensitive to increased loading. Yet, if pulse shape time histories of the upper frames, for the highly loaded rotor, are compared to the lower frames, for the moderately loaded rotor, one sees increases in the positive interactions, which are due to BVI, preceding the negative peak. This shows a greater sensitivity of BVI noise to increased loading in this flight regime. Note that for the highly loaded rotor at μ= 0.3, the first and dominant BVI interaction is equal, if not higher, in magnitude to the negative peak pressure due to the thickness noise. It is apparent that the BVI noise can substantially contribute to the acoustic radiation from the main rotor in the level flight (propulsive) mode as well as in low power descent, and in-plane as well as below the tip-path-plane.

To further determine the "delocalisation" advancing tip Mach number resulting from the transonic flow field, which marks the onset of HSI noise, the data were examined at higher advancing blade tip Mach numbers, up to M_{AT}= 0.93. In Figure 15, the negative peak acoustic pressures are plotted versus the advancing tip Mach number, using two scales: linear and logarithmic. Several level flight sweeps of both μ and M_H are presented, to better define the details of HSI noise trends. Four advance ratio sweeps are plotted: two conditions of high propulsive force operating at the nominal M_H at both a moderate and high loading (the same data presented in the previous figure), and two conditions of a moderate propulsive force operating at 10% above nominal M_H at both low and moderate loading conditions. Also, included are three M_H sweeps for advance ratios of 0.1, 0.2, and 0.3.

Examining the curves plotted by the log scale in Figure 15 which are labelled M_H sweeps, it can be seen that for the sweeps in which μ=0.1 and 0.2 there tends to be a greater variability with increasing M_H. This reinforces results found by Schmitz (Ref. 25), which shows that steady radiators of acoustic energy are more efficient generators of impulsive noise than unsteady ones of similar advancing tip Mach numbers. In interpreting this statement and relating to the measured data, at relatively high hover tip Mach numbers, say

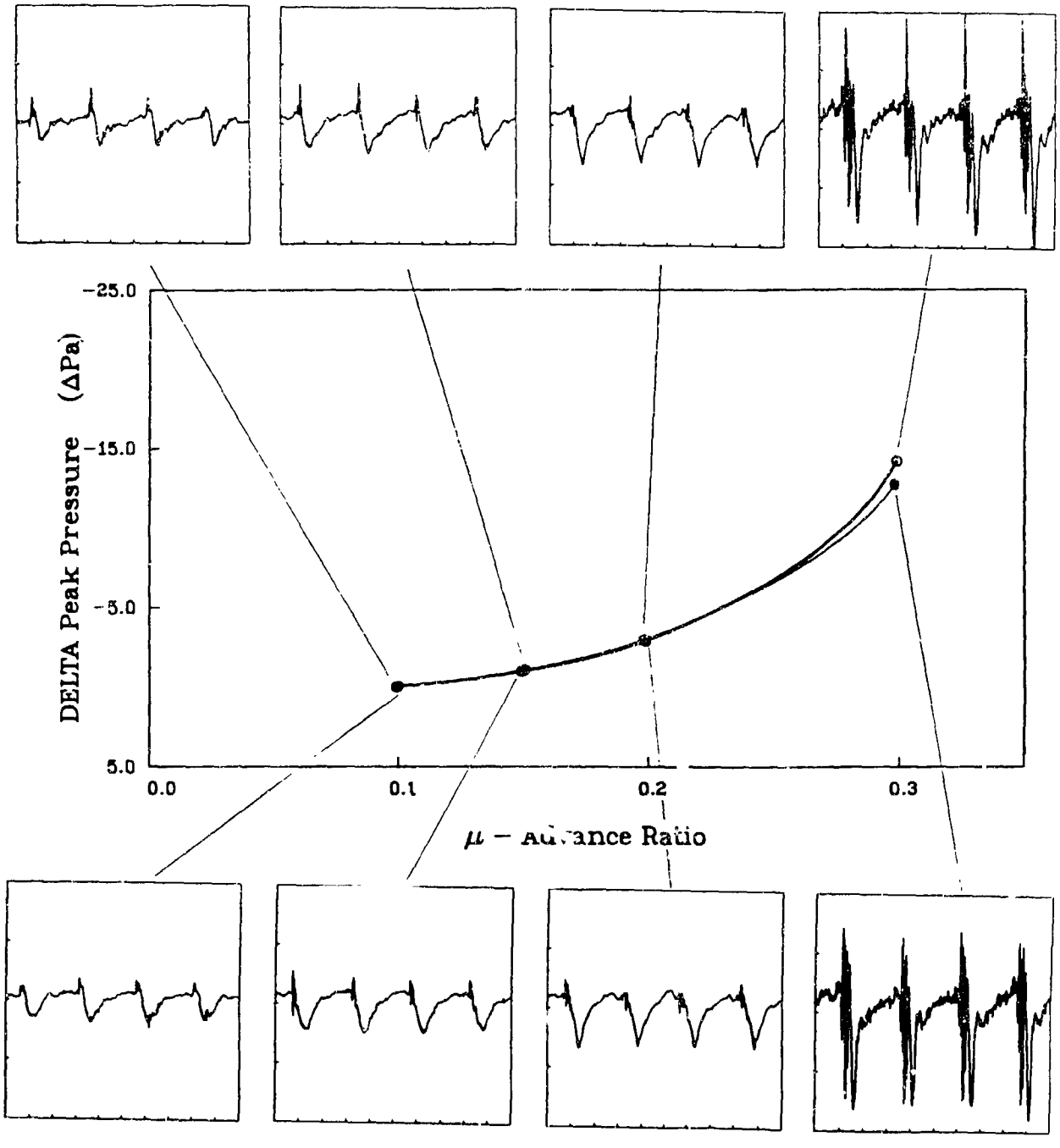

Figure 14. Acoustic levels in level forward flight.

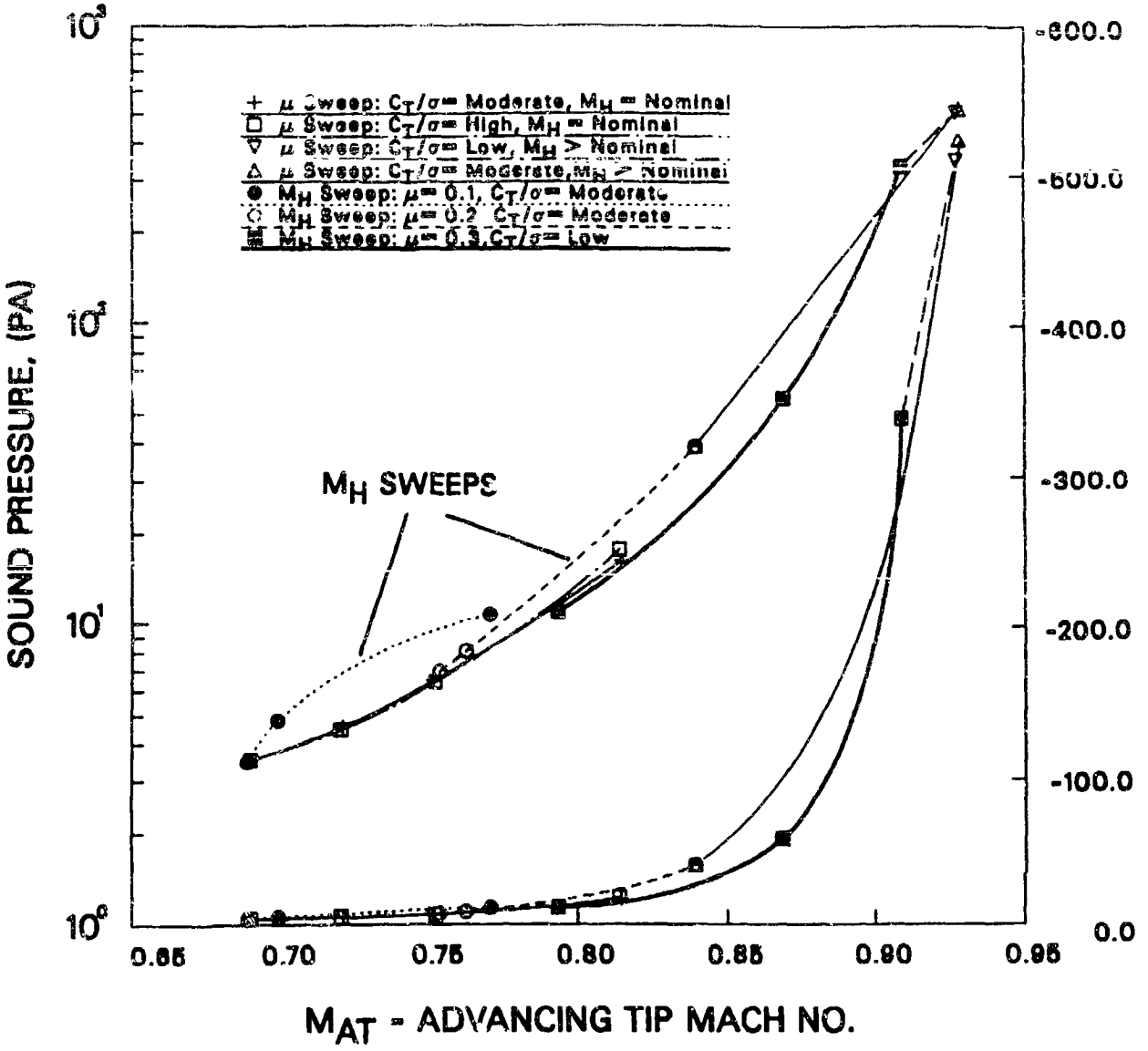

Figure 15. High Speed Impulsive(HSI) noise.

M_H ≈0.700, and a low advance ratio of μ=0.1, each rotor blade experiences only small variations in the local Mach number around the azimuth, implying that the "steady" compressible source mechanisms are the most likely radiators of far-field energy. At the same M_{AT}, but at a lower hover tip Mach number(M_H ≈0.640) and a higher adavance ratio(μ=0.20), significant variations in the local blade Mach number occur and can be expected to exert more influence on the radiated acoustic field. If we associate this with data, it reveals the "steady" compressible radiators of acoustic energy are more efficient radiators of impulsive noise than the unsteady ones of similar advancing tip Mach numbers and therefore result in the higher levels shown.

In Figure 15, the lower set of curves correspond to the linear scale at the right of the figure, which emphasizes the dramatic rise in the HSI noise due to compressibility as a result of increasing advancing tip Mach number. Similar to the findings for the AH-1 (Ref. 4), the logarithmic curves indicate that the rapid rate of increase in level near the onset of HSI noise does not continue indefinitely. The greatest slope is reached near the "delocalization" advancing tip Mach number and then levels off. The measured data ranged from a M_{AT}= 0.689 to 0.921. The delocalization advancing tip Mach number was identified as 0.889. At first this may seem unusual since the delocalization Mach number is similar to that of the AH-1 and the AH-1, being a two-bladed rotor system, not only has a higher individual blade loading but also a rectangular tip. However, the delocalization advancing tip Mach number is only indicating the onset of HSI noise, and provides no information concerning the magnitude. It is not the intention of this paper to make direct noise level comparisons of different rotor systems, but to study the sensitivities

of the acoustic parameters that are affected by rotor design.

To further examine some of the parameters affecting the delocalization advancing tip Mach number, a brief review of the available literature on HSI noise was made. Table I offers a summary of several other rotor systems that have documented the effects of HSI noise and identified the delocalization advancing tip Mach number. This brief summary of rotor parameters supports the analytical and experimental simulation of the delocalization phenomenon, which indicated the thinner the blade near the tip, the higher the Mach number at which delocalization appears. Although other factors such as blade twist, airfoil section geometry and tip sweep affect the tip relief and should thus be expected to also affect the delocalization Mach number, the contributing effects of these items cannot be determined. The available reported data seems to confirm that physical tip size is a key parameter for the onset of HSI noise. Both the Boeing Model 360 (Ref. 6) and DART blades (Ref. 26) have nearly the same relative tip thickness at maximum radius and resulting delocalization M_{AT} of 0.910-0.913. Similarly, both the UTC baseline swept tip and the AH-1 have much larger tip thicknesses relative to the former, and the data show a delocalization M_{AT} of 0.890. This indicates that the delocalization advancing tip Mach number is increased as a result of the reduced physical size of the blade tip.

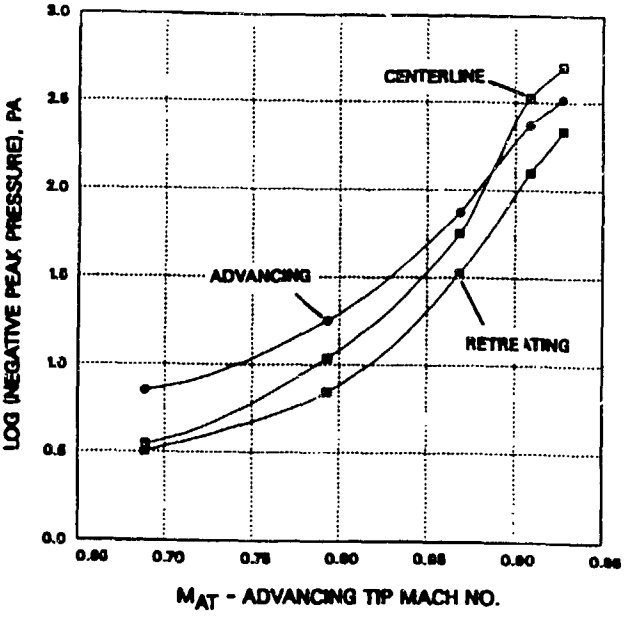

Figure 16. Measured directivity of HSI noise.

Data for the other inplane microphones, 30 degrees off to each side of the centerline, also indicated the same delocalization Mach number of 0.89. In Figure 16, the log of the peak negative acoustic pressures are plotted versus M_{AT} for the three inplane microphones. Below the delocalization M_{AT}, the highest impulsive noise levels are radiated upstream of the advancing side. Yet, beyond delocalization, the highest levels shift to directly upstream of the centerline of the rotor. This indicates the highly directional radiation pattern of impulsive noise sources.

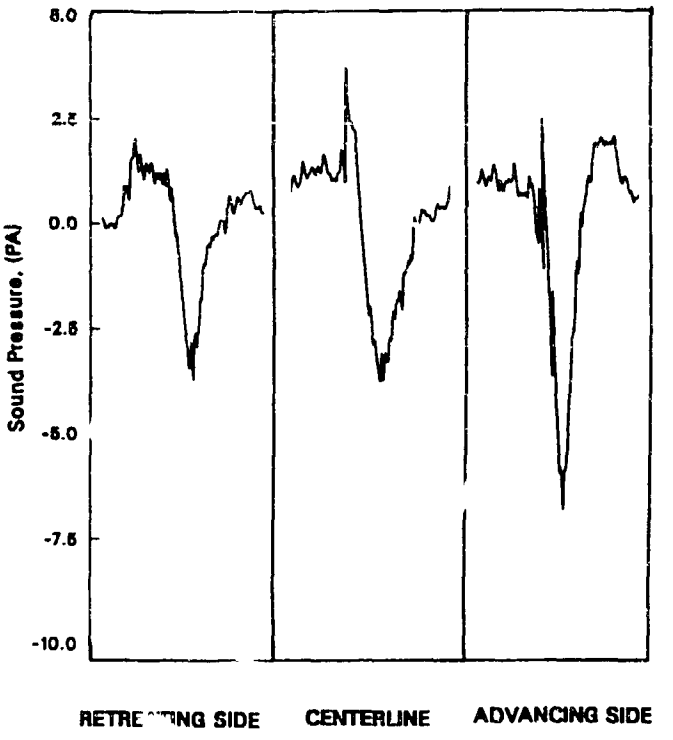

Figure 17a. Directivity time history of HSI noise for M_{AT}= 0.689.

In an effort to identify the noise mechanism responsible for the shift in directivity, the time histories of the test points of Figure 16 were examined. Figures 17a-17e show a quarter revolution of the time histories for the three inplane measurements in front of the rotor. In Figure 17a, the rotor is operating at M_{AT}=0.689. The flow is subsonic, and the negative pressure pulse is triangular in character. It reveals considerable influence from BVI sources. One can clearly see the effects of phasing between the BVI and thickness sources at these three different directivity angles. Upstream of the retreating side, the BVI signal is received forward sooner than the thickness source. However, upstream of the advancing side, the positive BVI impulse somewhat cancels the increasing negative pressure pulse due

to thickness noise, since the sign[illegible]re almost in phase but have opposing sign.

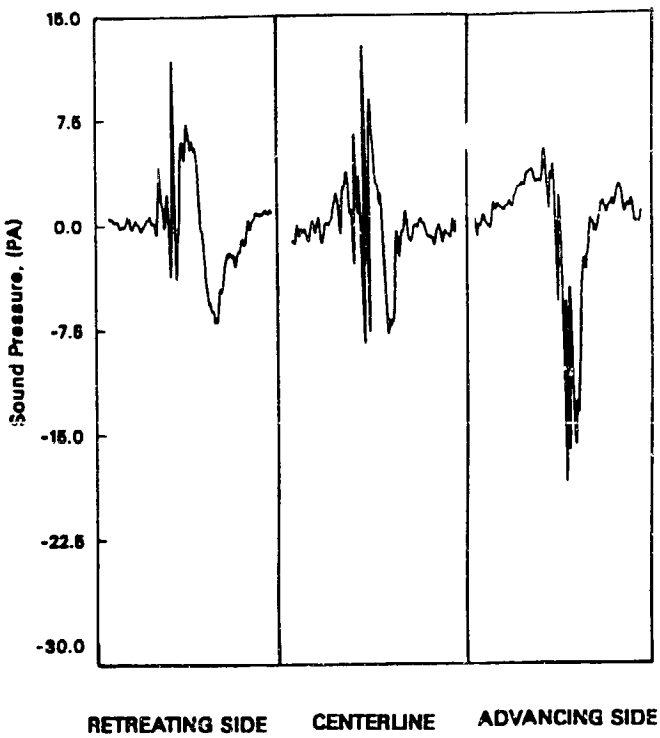

Figure 17b. Directivity time history of HSI noise for M_{AT}= 0.793.

In Figure 17b, the rotor is operating at M_{AT}= 0.793. The negative pressure pulse is still triangular in nature. There is evidence of BVI, yet not as dominant as in Figure 17a. The data of Figure 17c are from an operating condition of M_{AT}= 0.869, which is nearing the delocalisation value of 0.89, in which the signal has become somewhat "sawtooth" in character, typical of tra[illegible]onic flow. There again is contribution from BVI, but the thickness source is clearly dominant. Because BVI is evident, there is the possibility that it might have been the source of the shift in the HSI noise directivity. Yet, in Figures 17d and 17e, there is no clear indication [illegible]hat is the case.

In an effort to determine the mechanisms that alter the HSI noise directivity beyond delocalisation, several theories relating the geometrical setup and the shifting of the sou[illegible]ce locations were examined, but no clear reason can be provided at this time. [illegible]owever, it is speculated that it may be a functi[illegible]of the blade planform, in this case 20° blade tip sweep, [illegible]hich controls the highly directional source near the [illegible]ip. Further analysis of the acoustic data is required, in addi[illegible]on, to a detailed correlation of the acoustics and airloads, to more clearly define this effect.

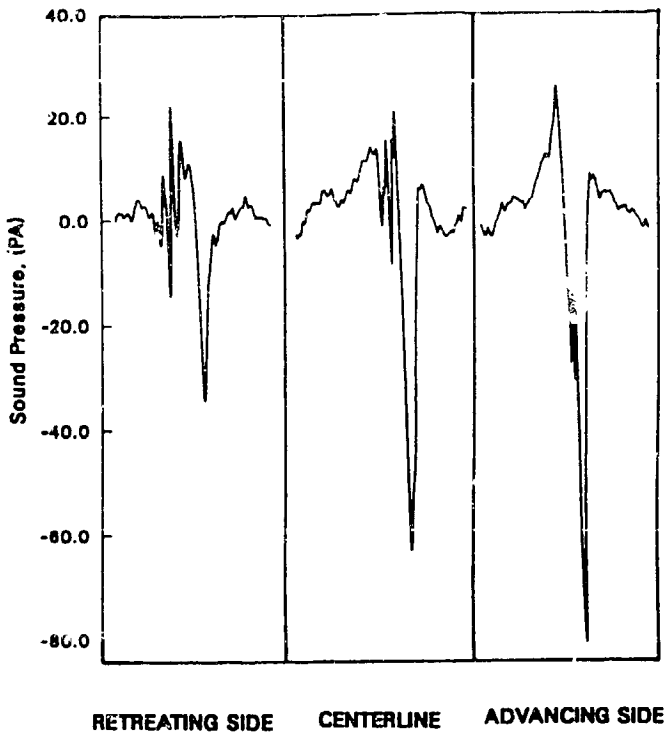

Figure 17c. Directivity time history of HSI noise for M_{AT}= 0.869.

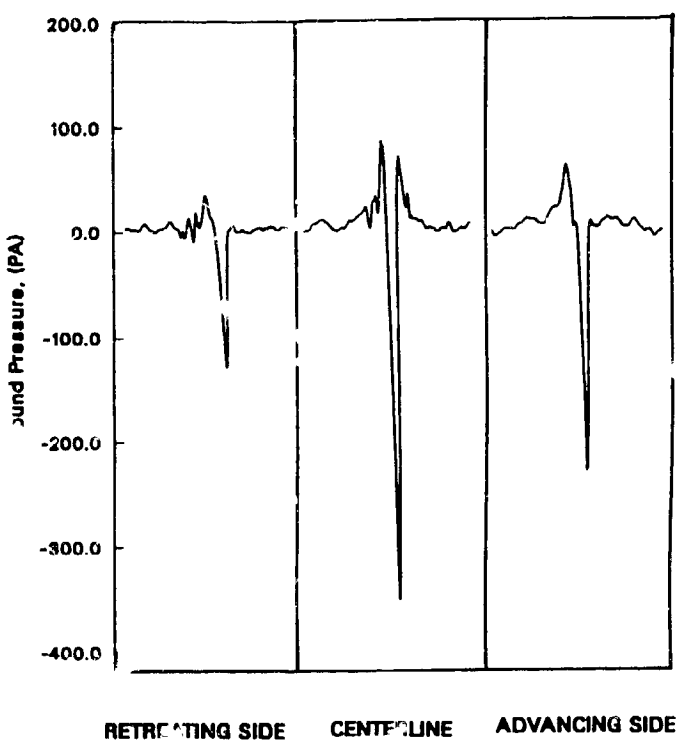

Figure 17d. Directivity time history of HSI noise for M_{AT}= 0.908.

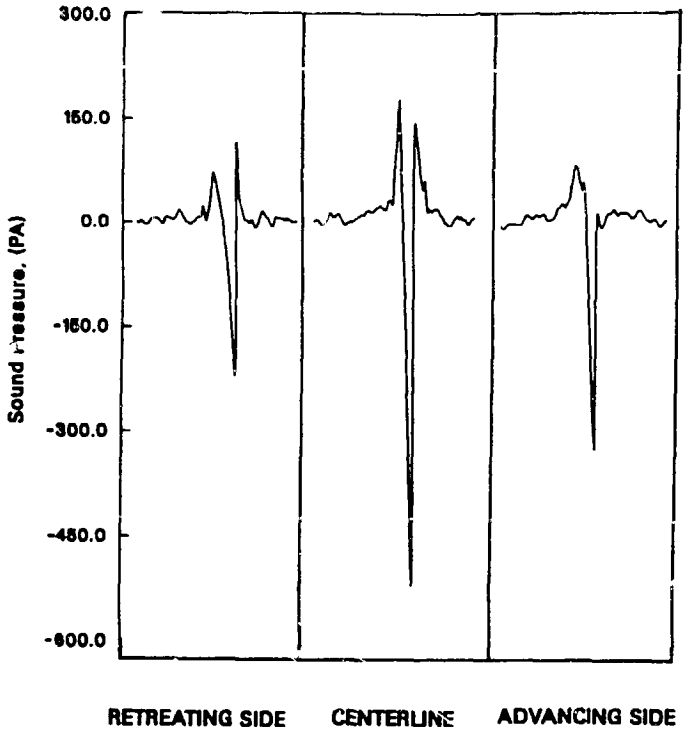

Figure 17e. Directivity time history of HSI noise for M_{AT}= 0.927.

Rotor System	% thickness	chord (in)	thickness (in)	$M_{Delocal}$
Boeing 360	9.0	1.60	0.1440	0.913
DART - swept	9.5	1.50	0.1425	0.910
UTC swept tip	9.5	[illegible]	0.3496	0.890
AH-1/OLS	9.7	4.09	0.3971	0.890

Table I. Summary of HSI noise results of several rotors.

CONCLUSIONS

Under the AATMR Program, several very comprehensive aero/acoustic databases of various configurations of the UTC scaled model rotor were established. The high quality acoustic, performance, dynamic and airloads data will help provide the foundation on which researchers will validate their computational methods necessary for the development of the next generation of advanced rotor systems.

For all of the configurations, the acoustic pressure field was measured by nineteen microphones, while steady state rotor balance data was simultaneously recorded. While four different rotor configurations were tested (instrumented main rotor, uninstrumented main and tail rotors, uninstrumented main rotor, and BERP-planform tip main rotor), only data from the baseline swept tip rotor are presented here. The acoustic data, with regard to both blade-vortex interaction and high speed impulsive noise mechanisms, show a sound, repeatable, high quality, which is expected to continue for the other tested configurations.

In the review and analysis of the data for the baseline swept tip rotor the following conclusions are made:

1.) The review of the acoustic data showed excellent repeatabilty throughout the testing phase of the program with minimal failure of any hardware.

2.) The uninstrumented and instrumented swept tip blade sets showed similar acoustic repeatability expanding the available number of test points and condition in acoustics as well as performance.

Blade-Vortex Interaction:

1) An acoustic simulation was performed for three typical approach maneuvers. It identified that significant variations in the noise field may result due to asimuthal (yaw angle) variation in the flight path during full-scale descent, as was expected due to the known highly directional nature of this mechanism.

2) The preliminary identification of the blade-vortex interaction locations seems to correlate well with simple reasoning for both parallel and oblique interactions.

3) The acoustic measurments have indicated BVI occurs in portions of forward flight not previously identified.

High Speed Impulsive:

1) The delocalization advancing tip Mach number is influenced by physical tip geometry as supported by the comparison of this rotor and other acoustic rotor databases.

2) The sound mechanisms in plane alter the directivity pattern beyond delocalisation. In this case, the maximum HSI lobe radiates forward at ψ=180°.

ACKNOWLEDGMENT

In such a large scale test , there are many people who deserve reco ion for a job well done. It was a very complex d ambitious test, performed and completed successfully through hard work and outstanding cooperation between government and industry. The authors would like to offer sincere thanks to their friends and colleagues at: the Army Aeroflightdynamics Directorate, United Technologies Research Center, Sikorsky Aircraft, NASA Ames and Langley Research Centers, and the DNW Foundation and its parent organizations, DLR and NLR. The authors are indebted to the following for their contributions made in acquiring the data presented in this paper:

Seth Dawson (AFDD - test direction), Peter Lorber (UTRC - aerodynamics and deputy test direction), Michael Pollack (Sikorsky - aerodynamics), Donald Boxwell (AFDD - acoustics), Chee Tung (AFDD - aerodynamics), Ruth Martin (NASA Langley - acoustics), Dave Jordan (NASA Ames - test operations), Lonnie Branum (AFDI - test operations), Jon Lautenschlager, Oswald Swenson (AFDD - instrumentation), Alfred Covino, David Crenella (UTRC - instrumentation), Michael Kodani, Alice Muldar (AFDD - computer support), Robert Grandle (NASA Langley - computer support), Thomas Miller (NASA Langley - acoustic technician), Raymond Lessard, Anthony Saccullo (Sikorsky - test operations), Benton Lau (NASA Ames - dynamics), Raj Shenoy (Sikorsky - acoustics), Robert Goodman, Kirk Frederickson (Sikorsky - dynamics), Brian Chan and Jack Ollila (AFDD - mechanical operations).

Management: Andrew Kerr, Yung Yu (AFDD), Jack Preisser (NASA Langley), Anton Landgrebe (UTRC), Robert Moffitt (Sikorsky).

REFERENCES

1 "Federal Registrar Noise Standards for Helicopters in the Normal, Transport, and Restricted Categories Final Rule," FAA 14CFR Part 21 and 36, Feb. 5, 1988.

2. Schmitz, F.H., Boxwell, D.A., Lewy, S., and Dahan, C., "A Note on the General Scaling of Helicopter Blade-Vortex Interaction Noise", American Helicopter Society 38th Annual National Forum, Anaheim, California, May 1982.

3. Splettstoesser, W.R., Schultz, K.J., Schmitz, F.H., and Boxwell,D.A.,"Model Rotor High Speed Impulsive Noise – Parametric Variations and Full-Scale Comparisons," American Helicopter Society 39th Annual National Forum, St.Louis, Missouri, May 1983.

4. Boxwell, D.A., Schmitz, F.H., Splettstoesser, W.R., and Schultz, K.J.,"Model Helicopter Rotor High-Speed Impulsive Noise: Measured Acoustics and Blade Pressures," NASA TM 85850, and USAAVRADCOM TR-83-A-14 September 1983.

5. Dadone, L., Dawson, S., Boxwell, D.A., and Ekquist, D., "Model 360 Rotor Test at DNW - Review of Performance and Blade Airloads Data," American Helicopter Society 43rd Annual National Forum, St.Louis, Missou ., May 1987.

6. Zinner, R.A., Boxwell, D.A., and Spencer, R.H., "Review and Analysis of the DNW/Model 360 Rotor Acoustics Data Base," Fifteenth European Rotorcraft Forum, Amsterdam, September 1989.

7. Dawson, S., Jordan, D., Smith, C., Ekins, J., Silverthorn, L., and Tuttle, B.,"Harp Model Rotor Test at DNW," American Helicopter Society 45th Annual National Forum, Boston, Massachusetts, May, 1989.

8. Lorber, P.F., Stauter, R.C., and Landgrebe, A.J., "A Comprehensive Hover Test of the Airloads and Airflow of an Extensively Instrumented Model Helicopter Rotor," American Helicopter Society 45th Annual National Forum, Boston, Massachusetts, May 1989.

9. Lorber, P.F., Stauter, R.C., Pollack, M.J., and Landgrebe, A.J., "A Comprehensive Hover Test of the Airloads and Airflow of an Extensively Instrumented Model Helicopter Rotor" (Volumes I-IV), USAAVSCOM TR 89-D-28A,B,C,D, U.S. Army AATD, Ft Eustis VA, 1990.

10. Yu, Y.H , Liu, S.R., Landgrebe, A.J., Lorber, P.F., Jordan, D.E Pollack, M.J., Martin, R.M., "Aerodynamic and Acoustic Test of a United Technologies' Model Scale Rotor at DNW," American Helicopter Society 46th Annual Forum, Washington DC, May 1990.

11. Lorber, P.F., "Aerodynamic Results of a Pressure-Instrumented Model Rotor Test at the DNW," American Helicopter Society 46th Annual Forum. Washington DC, May 1990.

12. Schmitz, F.H., and Yu, Y.H., "Helicopter Impulsive Noise: Theoretical and Experimental Status," Journal of Sound and Vibration Vol.109(3), 1986, pg.361-422.

13. Boxwell, D.A., Yu, Y.H , and Schmitz, F.H., "Hovering Impulsive Noise: Measured and Calculated Results," Vertica 3.35-45,1979.

14. Splettstosser, W.R., Schultz, K.J., Schmitz, F.H., and Boxwell, D.A., "Helicopter Model Rotor Blade-Vortex Interaction Impulsive Noise – Scalability and Parametric Variations," Tenth European Rotorcraft Forum, Hague, Netherlands, August 1984.

15. Egolf, T.A., and Landgrebe, A.J.,"Helicopter Rotor Wake Geometry and Its Influence in Forward Flight. Volume I - Generalized Wake Geometry and Wake Effects on Rotor Airloads and Performance, Volume II - Wake Geometry Charts," NASA CR 3726 and 3727, June 1983.

16. Splettstoesser, W.R., Schultz, K.J., and Martin, R.M., "Rotor Blade-Vortex Interaction Impulsive Noise Source Identification and Correlation with Rotor Wake Predictions," Tenth European Rotorcraft Forum, Hague, Netherlands, August 1984.

17. Joshi, M.C., Liu, S.R., and Boxwell, D.A., "Prediction of Blade-Vortex Interaction Noise, "American Helicopter Society 43rd Annual National Forum, St. Louis, Missouri, May 1987.

18. Ziegenbein, P.E., and Oh, B.K.,"Blade-Vortex Interaction Noise Prediction Using Measured Blade Surface Pressures," AHS Specialists' Meeting on Aerodynamics and Aeroacoustics, Arlington, Texas, February 1987.

19. Martin, R.M., and Hardin J.C.,"Spectral Characteristics of Rotor Blade-Vortex Interaction Noise," AIAA 25th Aerospace Sciences Meeting," Reno, Nevada, January 1987.

20. Nakamura, Y.,"Prediction of Blade-Vortex Interaction from Measured Blade Pressure," Seventh European Rotorcraft and Power Lift Aircraft Forum, Garmisch - Partenkirchen, Federal Republic Germany, September 1981.

21. J.C.A van Ditshuizen et al.,"Acoustic Capabilities of the German-Dutch Wind Tunnel," AIAA Paper 83-0146,1983.

22. J.C.A van Ditshuizen,"Compilation of Calibration Data of the German-Dutch Wind Tunnel," DNW Report MP-82.01, 1982.

23. Martin, R.M. Personal communication. Novmber, 1989.

24. George, A.R., and Chang, S.B., "Noise Due to Transonic Blade-Vortex Interaction," American Helicopter Society 39th Annual National Forum, St. Louis, May 1983.

25. Schmitz, F.H., Boxwell, D.A., and Vause, C.R.,"High Speed Helicopter Impulsive Noise," Journal of American Helicopter Society 22, 1977.

26. Purcell, T.W., "A Prediction of High-Speed Rotor Noise," AIAA 12th Aeroacoustic Conference, San Antonio, TX, April 1989.

27. Fitzgerald, J., and Kohlhepp, F., "Research Investigation of Helicopter Main Rotor/Tail Rotor Interaction Noise " NASA Contractor Report 4143, May 1988.